

Role of $f - d$ exchange interaction and Kondo scattering in the Nd-doped pyrochlore iridate $(\text{Eu}_{1-x}\text{Nd}_x)_2\text{Ir}_2\text{O}_7$

Sampad Mondal,^{1,2,3,*} M. Modak,² B. Maji,^{2,4} Mayukh K. Ray,⁵ S. Mandal,²
Swapan K. Mandal,¹ M. Sardar,⁶ and S. Banerjee^{2,†}

¹*Department of Physics, Visva-Bharati, Santiniketan 731235, India*


²*Saha Institute of Nuclear Physics, HBNI, 1/AF Bidhannagar, Kolkata 700064, India*

³*Ramsaday College, Amta, Howrah 711401, India*

⁴*Acharya Jagadish Chandra Bose College, 1/1B, A. J. C. Bose Road, Kolkata 700020, India*

⁵*Institute of Solid State Physics, University of Tokyo, Kashiwa 277-8581, Japan*

⁶*Material Science Division, Indira Gandhi Centre for Atomic Research, Kalpakkam 603102, India*

 (Received 9 March 2020; revised 14 August 2020; accepted 30 September 2020; published 26 October 2020)

We report a study of magnetization, resistivity, magnetoresistance, and specific heat of the pyrochlore iridate $(\text{Eu}_{1-x}\text{Nd}_x)_2\text{Ir}_2\text{O}_7$ with $x = 0.0, 0.5$ and 1.0 , where spin-orbit coupling, electronic correlation, magnetic frustration, and Kondo scattering coexist. The metal insulator transition temperature (T_{MI}) decreases with increase in Nd content, but always coincides with the magnetic irreversibility temperature (field-induced moment). Resistivity below T_{MI} does not fit with either activated (gap) or any power-law (gapless) dependence. The Curie constant shows the surprising result that Nd induces singlet correlation (reduction of paramoment) in the Ir sublattice. Magnetoresistance is negative at low temperatures below 10 K and increases strongly with increase in x , and varies quadratically with field switching over to a linear dependence above 50 kOe. Low-temperature specific heat shows a Schottky peak, coming from Nd moments, showing the existence of a doublet split in the Nd energy level, arising from the $f - d$ exchange interaction. All materials show the presence of a linear specific heat in the insulating region. The coefficient of linear specific heat for $x = 0.0$ does not vary with the external magnetic field, but varies superlinearly for $x = 1.0$ materials. We argue that linear specific heat probably rules out weakly correlated phases such as Weyl fermions. We propose that with the introduction of Nd at the Eu site, the system evolves from a chiral spin liquid with gapless spinon excitations with a very small charge gap to a Kondo-type interaction superposed on a chiral spin liquid coexisting with long-range antiferromagnetic ordering. A huge increase of magnetoresistance with increase in Nd concentrations shows the importance of Kondo scattering in the chiral spin-liquid material by rare-earth moments.

DOI: [10.1103/PhysRevB.102.155139](https://doi.org/10.1103/PhysRevB.102.155139)

I. INTRODUCTION

The focus in condensed-matter physics nowadays is in understanding the emergence of Dirac-like fermions under various circumstances [1]. A common theme is spin-orbit entanglement produced by spin-orbit interaction, influencing electronic and magnetic transitions [2]. The topology of the band structure is also important and it was suggested that in the weak-correlation regime, quadratic band touching at some points in the Brillouin zone can lead to a large number of phases related to topological insulators, such as three-dimensional Dirac [3] and Weyl [4] semimetals and an axion insulator [5]. Specifically in the magnetically ordered phase, where time-reversible symmetry is broken but inversion symmetry is preserved, the pairs of quadratic band touching points lead to a linearly dispersing Dirac fermion type spectrum, along with definite chirality, i.e., $\vec{k} \cdot \vec{\sigma} = \pm 1$, where \vec{k} and $\vec{\sigma}$ are unit vectors along the momentum and spin of the

electrons. This leads to many interesting properties such as the Hall effect without external magnetic field, as well as negative/positive magnetoresistance when the electric field and magnetic fields are parallel/perpendicular [6–8].

In the strong-correlation limit, the already narrow bands due to spin-orbit coupling may open up a gap. With an increase in the local Coulomb correlation, pairs of opposite chirality Weyl points move towards the Brillouin-zone boundary and annihilate pairwise to open up a gap, forming spin-orbit assisted Mott insulators [9]. Owing to frustration in the magnetic exchange interaction (like in pyrochlores), one might get either metallic or insulating spin-liquid phases [10]. This spin-liquid phase may also be chiral, but this time chirality is defined in terms of real-space localized spin variables such as $\vec{S}_i \cdot \vec{S}_j \times \vec{S}_k$ developing nonzero expectation values, where \vec{S}_i, \vec{S}_j , and \vec{S}_k are spins at sites i, j , and k in a triangular plaquette. Interestingly, this phase can also give the anomalous Hall effect (without external magnetic field) and negative magnetoresistance such as Weyl fermions if the transport gap is small.

To study the combined effect of spin-orbit coupling and electronic correlation, the $5d$ iridium oxides, such as

*sampad100@gmail.com

†sangam.banerjee@saha.ac.in

pyrochlore iridates $\text{Ln}_2\text{Ir}_2\text{O}_7$ where Ln is a lanthanide, are the best candidates. The interpenetrating corner-sharing tetrahedral structure is favorable to form a narrow flat band that enhances the effect of electron correlation and spin-orbit coupling (SOC), and both of these energies are comparable to the band width. They also have a structure where antiferromagnetic interaction between magnetic ions is frustrated. These materials are proposed [11] to have many interesting topological phases and are being pursued by experimentalists to discover interesting properties of matter.

$\text{Ln}_2\text{Ir}_2\text{O}_7$ (R =rare earth) have shown many interesting transport and magnetic properties [12–14], and show a transition from incoherent and strongly correlated metal (at high temperature) to an antiferromagnetically ordered insulator/semimetal (at low temperature), except when $\text{Ln}=\text{Pr}$. The transition temperature decreases as the ionic radius of the rare-earth atom increases [14]. A metal to insulator/semimetal transition is reminiscent of the Mott-Hubbard transition, but with the added complexity that (1) spin and orbital degrees of freedom are entangled due to spin-orbit coupling, (2) both transition metal and rare-earth sublattices are magnetically frustrated, and (3) there is local Kondo coupling ($f-d$ exchange interaction) between localized rare-earth moments and the transition metal electrons. In $\text{Eu}_2\text{Ir}_2\text{O}_7$, we can avoid $f-d$ exchange interaction because the net moment of Eu^{3+} is zero. This is a suitable system to study the effect of both SOC and electronic correlation. A continuous phase transition from paramagnetic metal to antiferromagnetic insulating state was observed in single crystals [15]. Low-frequency optical conductivity [16] increases linearly with frequency. This is consistent with a Dirac-like spectrum with density of states varying linearly with energy, suggesting that $\text{Eu}_2\text{Ir}_2\text{O}_7$ is a Weyl semimetal. From analysis of resistivity, Tafti *et al.* [17] have suggested that $\text{Eu}_2\text{Ir}_2\text{O}_7$ goes from paramagnetic metal to Weyl semimetal (in an intermediate-temperature window) and, finally, to an antiferromagnetic insulator at the lowest temperature. Paradoxically, in the low-temperature region (below 10 K), the optical conductivity was also found to be proportional to frequency. When the rare-earth sites have moment (such as Nd), the $f-d$ exchange interaction (Kondo) can mediate a Ruderman-Kittel-Kasuya-Yosida (RKKY)-type exchange interaction between the localized rare-earth moments, which, along with the superexchange interaction between themselves, may induce the ordering of the Nd sublattice system. The magnetic ordering of the Nd subsystem can, in turn, modify the electronic structure of the Ir subsystem, promoting many exotic quantum correlated phenomena. Even when Nd moments are not ordered yet, the Kondo scattering between the f and d electrons can profoundly affect the electronic properties of the Ir electrons. The Weyl fermion is a weak-correlation concept and is unlikely to survive with an increase in correlation. It has been argued [18] that the $f-d$ interaction, along with strong correlation, can again stabilize the Weyl semimetal phase. Polycrystalline $\text{Nd}_2\text{Ir}_2\text{O}_7$ shows a metal insulator transition at 33 K [19]. Raman scattering confirms that there is no structural change accompanying the metal insulator transition [20]. Optical [21], transport [22], and photoemission [23] experiments suggest a gapped insulating ground state in $\text{Nd}_2\text{Ir}_2\text{O}_7$. The $\text{Nd}_2\text{Ir}_2\text{O}_7$ compound

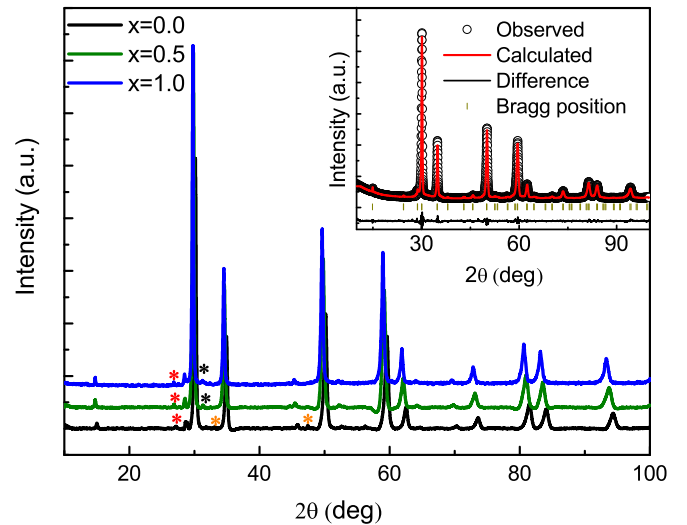


FIG. 1. Room-temperature x-ray diffraction pattern for the sample $(\text{Eu}_{1-x}\text{Nd}_x)_2\text{Ir}_2\text{O}_7$, where $x = 0, 0.5, 1.0$, and red, orange, and black stars indicate the impurity phase due to nonreacting IrO_2 , Eu_2O_3 , and Nd_2O_3 , respectively. Inset: Rietveld refinement for an $x = 0.0$ compound, where scattered data are observed and the solid line is a fit to the data.

develops a long-range antiferromagnetic all-in-all-out (AIAO) ordering of the Nd moments [24] below 15 K (though the magnitude of the ordered Nd moments is very small), confirmed by an inelastic neutron-scattering measurement [25]. Long-range antiferromagnetic ordering is destroyed by the applied magnetic field, producing a field-induced insulator to metal transition [22,26]. We have prepared polycrystalline $\text{Eu}_{2(1-x)}\text{Nd}_x\text{Ir}_2\text{O}_7$, with $x = 0.0, 0.5$ and 1.0 , and have studied resistivity, magnetoresistance, magnetization, and specific heat with and without a magnetic field.

II. EXPERIMENTAL DETAILS

All the polycrystalline samples were prepared by the solid-state reaction method. High-purity ingredient powder Eu_2O_3 , IrO_2 , and Nd_2O_3 were mixed in a stoichiometric ratio and ground well. After pressing the mixture powder into pellet form, it is heated at 1373 K for three days with several intermediate grindings. All the samples were characterized by powder x-ray diffraction (XRD). The room-temperature XRD measurement was taken with an x-ray diffractometer with $\text{Cu K}\alpha$ radiation. The structural parameter was determined using the standard Rietveld technique with the FULLPROF software package. The magnetic measurement was taken using the superconducting quantum interference device magnetometer (SQUID-VSM) of Quantum Design in the temperature range 3–300 K. Electrical, magnetic, and thermal transport measurements were carried out using the Physical Properties Measurement System (PPMS).

III. EXPERIMENTAL RESULTS

The room-temperature XRD patterns for the samples $(\text{Eu}_{1-x}\text{Nd}_x)_2\text{Ir}_2\text{O}_7$, with $x = 0.0, 0.5, 1.0$, are shown in Fig. 1. There is no modification of the XRD pattern, but the peaks

shift to lower angles with Nd substitution at the Eu site. The observed data of all samples are refined on the basis of cubic structure with space group $Fd\bar{3}m$ by the Rietveld refinement method. Refinement of the $x = 0.0$ compound is shown in the inset of Fig. 1. All the samples are nearly in the pure phase, except some minor impurity phases (nonreacting oxide) which are marked with a star. In the $x = 0.0$ compound, the impurity phases due to nonreacting oxide IrO_2 and Eu_2O_3 are 0.62% and 0.89%, respectively, and the IrO_2 , Nd_2O_3 impurity phases in the $x = 0.5$ and 1.0 compounds are 0.72%, 0.69% and 0.78%, 0.82%, respectively. The obtained lattice parameters from the Rietveld refinement for the $x = 0, 0.5$, and 1.0 compounds are 10.3142, 10.3472, and 10.3858 Å, respectively. The increase of the lattice parameter with Nd doping indicates that Eu^{3+} is substituted by the larger ionic radius Nd^{3+} .

Figure 2(a) shows the temperature-dependent resistivity of the sample $(\text{Eu}_{1-x}\text{Nd}_x)_2\text{Ir}_2\text{O}_7$, with $x = 0, 0.5$, and 1.0, from 3 to 300 K. All samples show the metal to insulator transition (MIT), i.e., $\frac{d\rho}{dT}$ changes from positive to negative below the MIT temperature (T_{MI}). The observed MIT temperatures of $x = 0, 0.5$, and 1.0 compounds are 120, 95, and 35 K, respectively. Both T_{MI} as well as the resistivity in the entire temperature range decrease with Nd doping. This is consistent with earlier observations [14] that T_{MI} decreases with an increase in the rare-earth ionic size. From Rietveld refinement, we find that a higher ionic radii ion that is Nd doped at the Eu site increases the bond angle between Ir-O-Ir, which increases the Ir-O orbital overlap leading to an increased Ir-Ir hopping matrix element, i.e., Ir t_{2g} band width [27]. The MI transition gives the appearance of a straightforward Mott-Hubbard transition (competition between hopping matrix element and local Hubbard repulsion), but attempts to fit the resistivity in the insulating phase with the activated form (with a gap) fail, as it shows that the gap is temperature dependent with a maximum below T_{MI} and very small near 3 K and T_{MI} [see the inset in Fig. 2(b)]. On the other hand, μSR experiments in Eu and Nd compounds show a continuous rise of well-defined muon precession frequency below T_{MI} [28,29], indicating long-range magnetic ordering into a commensurate structure, as is expected in an antiferromagnetically ordered Mott insulating state. Antiferromagnetic ordering can emerge in weak-coupling (small Hubbard U) theories, such as in a Slater antiferromagnetic state, but the temperature dependence of the transport gap is disturbing. It has been suggested theoretically [30] that arbitrarily small antiferromagnetic ordering of Ir electrons can convert quadratic band touching points into a Weyl semimetal phase with Dirac cone linear dispersions at some points on the Brillouin zone. Optical conductivity in $\text{Eu}_2\text{Ir}_2\text{O}_7$ measured at 7 K shows [16] a linear dependence on the frequency at the lowest frequencies, consistent with the density of states $\rho(E) \propto |E - E_F|$ expected out of a Weyl semimetal. This should also mean that the low-temperature resistivity must vary with temperature as $\frac{1}{T}$ and was predicted theoretically [1]. We find that the resistivity of none of the samples varies in a power-law ($\frac{1}{T^\alpha}$) fashion from 3 K to T_{MI} . A single-crystal resistivity measurement [15] of $x = 0.0$ showed a surprising result, i.e., the temperature dependence of the resistivity of all single crystals (made in the same batch) coincides above T_{MI} , while below T_{MI} , there are wide discrepancies in the resistivity values between samples,

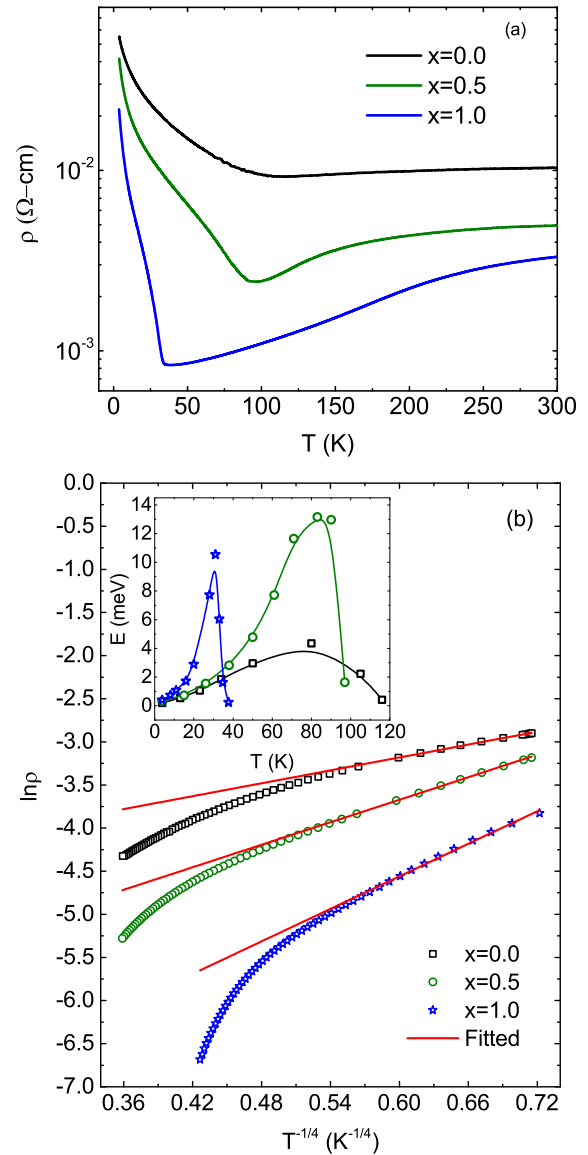


FIG. 2. (a) Temperature-dependent resistivity measured with the temperature range 3.8–300 K. (b) Fitting of resistivity below the MIT for the compounds $(\text{Eu}_{1-x}\text{Nd}_x)_2\text{Ir}_2\text{O}_7$, where $x = 0, 0.5$, and 1.0. Inset: Variation of the charge gap (E) with temperature for all the samples.

and the residual resistivity at the lowest temperature varies by four orders of magnitude between samples. There are two sources of possible disorder: (1) a slight difference in oxygen concentration [15] and (2) an interchange of a small fraction of Eu and Ir sites [31]. Both have the net effect of doping the hole in the half-filled Ir subsystem. It is found that more stoichiometric materials have larger residual resistivity [15]. Sr doping in $\text{Eu}_2\text{Ir}_2\text{O}_7$ [32] and Ca doping in $\text{Nd}_2\text{Ir}_2\text{O}_7$ [33] leads to a reduction of T_{MI} , and both systems above T_{MI} show non-Fermi-liquid properties. More importantly, it is found [34] that $\text{Nd}_2\text{Ir}_2\text{O}_7$ fragments into magnetic domains separated by domain walls, and the domain-wall region has much lower resistivity than within the magnetic domains, i.e., the measured conductivity is that of the domain walls and not of the bulk. Assuming the antiferromagnetic regions as

TABLE I. Fitting parameter T_0 and temperature range obtained from the VRH model for the sample $(\text{Eu}_{1-x}\text{Nd}_x)_2\text{Ir}_2\text{O}_7$.

Sample	Temperature range (K)	$T_0(\text{K})(10^3)$
$x = 0.0$	3.8–14	0.038
$x = 0.5$	3.8–19	0.357
$x = 1.0$	3.8–12	1.559

topological insulators, the domain walls might have gapless surface states. It is to be noted that topological insulator and Weyl metal/semimetals arise due to chirality in momentum space. Moreover, optical [21], transport [22], and photoemission [23] experiments suggest a gapped insulating ground state in $\text{Nd}_2\text{Ir}_2\text{O}_7$. In view of the fact that there is unavoidable nonstoichiometry as well as domain formation in these materials, it is worthwhile to look at a theoretical [35] analysis of the disordered Weyl metals. The main conclusions from the theoretical calculations are (1) resistivity crosses over to $\frac{1}{T^{0.5}}$ from $\frac{1}{T}$ (for clean Weyl metal), and (2) the magnetoresistance at low field is positive (antilocalization because of spin-orbit coupling) and switches over to negative at higher field. Both of these are not observed in our materials.

On the other hand, we find that resistivity of all three samples can be fitted to the three-dimensional Mott variable-range hopping (VRH) model [36],

$$\rho = \rho_0 \exp[(T_0/T)^{1/4}], \quad (1)$$

where $T_0 = \frac{21.2}{N(E_F)\xi^3}$, and $N(E_F)$ and ξ are the density of states at the Fermi level and localization length, respectively. It fits the data well but only within a limited range of temperature (less than one order of magnitude, i.e., from 3 to 20 K only). T_0 increases with Nd doping, as shown in Table I. Assuming that the density of states does not vary much between the samples, it shows that ξ decreases with increase in Nd concentration, but since the fit is over such a small range of temperatures, we do not force this point (strong localization).

Figures 3(a)–3(c) show the temperature-dependent susceptibility of the samples in the zero field cooled (ZFC) and field cooled (FC) protocols, measured under applied magnetic field of 1 kOe within a temperature range 3–300 K. M_{ZFC} for the parent compound increases with decrease in temperature with a weak magnetic anomaly close to 120 K. M_{FC} merges with M_{ZFC} up to temperature 120 K, below which there is a bifurcation between M_{ZFC} and M_{FC} . The magnetic irreversibility start at $T_{\text{irr}} \approx 120$ K. Resonant x-ray diffraction (RXD) and μSR (muon spin rotation and relaxation) measurements have shown that below T_{irr} , Ir moments order antiferromagnetically (AIAO) [28,37], though it needs emphasis that the magnitude of the ordered moment is very small. As the interval energy level of Eu^{3+} and Sm^{3+} , between the ground state and the successive first-excited state that is comparable with the thermal energy at room temperature, they show temperature-dependent Van Vleck susceptibility [38]. To obtain the contribution of the Ir moment in the parent compound, we subtracted the Van Vleck susceptibility χ_{VV} due to the Eu^{3+} ion from χ . Temperature-dependent χ_{VV} was calculated by using $\lambda = 400$ K [38], and is shown in Fig. 3(a) by the dotted line. The doped sample also shows bifurcation

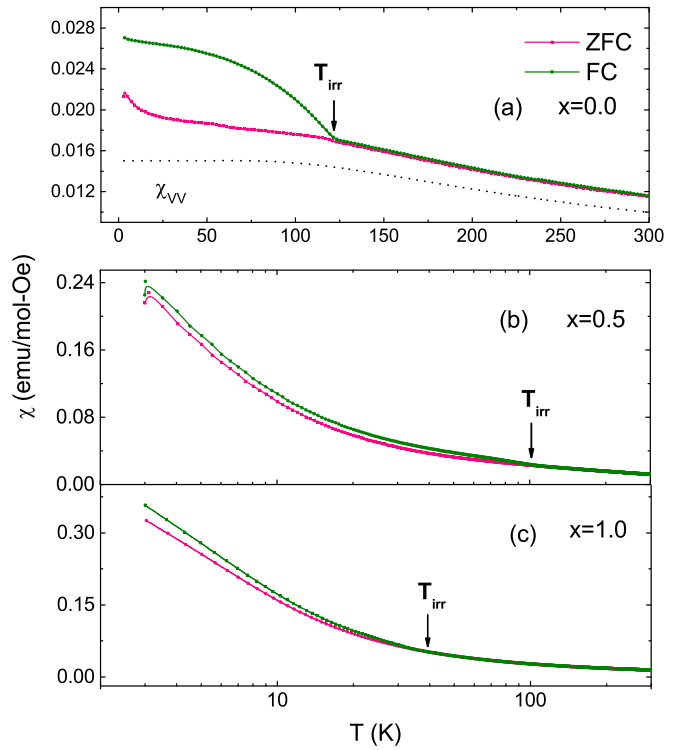


FIG. 3. (a)–(c) Temperature-dependent magnetization measured at 1 kOe in the ZFC FC protocol for $(\text{Eu}_{1-x}\text{Nd}_x)_2\text{Ir}_2\text{O}_7$, where $x = 0, 0.5, 1.0$, and the dotted line for the $x = 0$ compound represents Van Vleck susceptibility χ_{VV} of the Eu^{3+} ion.

but lesser in magnitude compared to the parent compound. T_{irr} decreases with Nd concentration. T_{irr} for the $x = 0, 0.5$, and 1.0 samples are 120, 100, and 38 K, respectively, and are identical to T_{MI} . No magnetic anomaly of M_{ZFC} is seen in the doped samples down to the lowest temperature.

Figures 4(a)–4(c) show temperature-dependent inverse susceptibility in the entire temperature region, fitted in the temperature range 140–290 K with Curie-Weiss law $\chi = \frac{C}{T - \theta_p}$, where θ_p is the Curie-Weiss temperature, the Curie constant $C = \frac{N_A \mu_{\text{eff}}^2}{3K_B}$, and μ_{eff} is the effective param-

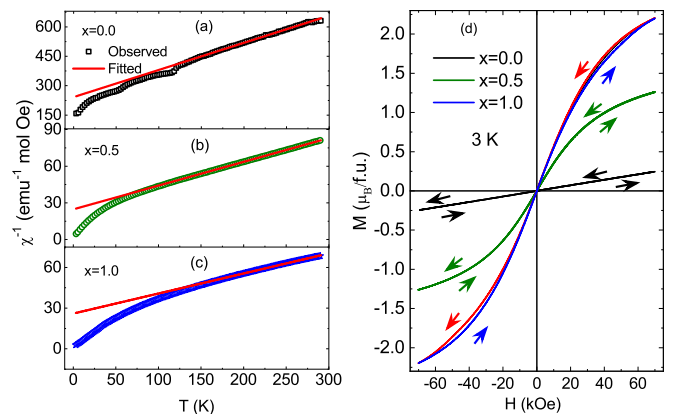


FIG. 4. (a)–(c) Temperature-dependent inverse susceptibility and (d) isothermal magnetization at 3 K for $(\text{Eu}_{1-x}\text{Nd}_x)_2\text{Ir}_2\text{O}_7$, where $x = 0, 0.5$, and 1.0 .

TABLE II. θ_p , μ_{eff} for the $(\text{Eu}_{1-x}\text{Nd}_x)_2\text{Ir}_2\text{O}_7$ system.

Sample	θ_p (K)	μ_{eff} ($\mu_B/\text{f.u.}$)
$x = 0.0$	-175	2.40
$x = 0.5$	-127	6.41
$x = 1.0$	-175	7.35

agnetic moment. θ_p , μ_{eff} for all the samples are shown in Table II. At the high-temperature region (140–290 K), all the materials show Curie-Weiss susceptibility. As the temperature decreases, inverse susceptibility deviates from a linear dependence with changing its slope below 140 K. At very low temperatures, inverse susceptibility starts bending down towards low values, presumably because of the pure Curie contribution coming from some noninteracting isolated moments. All the samples show negative θ_p at the high-temperature region, indicating antiferromagnetic interaction. It is hard to determine the exact moment contribution of Nd^{3+} and Ir^{4+} from this measurement. If we assume the contribution of the magnetic moment for Nd^{3+} ($3.57 \mu_B$) from the reported $\text{Nd}_2\text{Sn}_2\text{O}_7$ [39] where Sn^{4+} has no moment, then the contribution of the Ir local moment in the metallic phase for $x = 0.5$ and 1.0 compounds is $1.42 \mu_B$ and $0.11 \mu_B$, respectively. This indicates that the Ir moment decreases with Nd doping. Decrease of the Ir paramagnet in doped materials indicates the occurrence of a strong singlet correlation between the Ir moments by $f - d$ exchange interaction with the Nd moments.

Isothermal magnetization data ($M-H$) taken at 3 K, up to magnetic field 70 kOe, of all samples are shown in Fig. 4(d). The parent compound shows linear behavior without any magnetic saturation up to magnetic field 70 kOe. The $x = 0.5$ and 1.0 compounds show nonlinear behavior without any magnetic saturation up to field 70 kOe. The magnetic moment increases with Nd doping and the moment at 70 kOe, of the $x = 0.0, 0.5$, and 1.0 compounds, is 0.246, 1.263, and $2.20 \mu_B/\text{f.u.}$, respectively. This low value compared to the paramagnetic moments given in Table II clearly indicates the onset of antiferromagnetic ordering. A close view of Fig. 4(d) shows that the coercive field (H_C) and remanent magnetization (M_r) for the $x = 0.0, 0.5$, and 1.0 compounds, are 0.0, 30, 20 Oe and 0.0, 4.16×10^{-5} , and $8.29 \times 10^{-4} \mu_B/\text{f.u.}$, respectively.

Magnetoresistance (MR) defined by $[\rho_H - \rho_0]/\rho_0$, where ρ_0 and ρ_H are resistivity without and with applied field, is shown in Figs. 5(a)–5(c). Figure 5(a) shows magnetic field dependent MR at 3 K for all the samples. The parent compound shows very small negative MR (0.6% at 90 kOe), which varies quadratically at low field [see inset of Fig. 5(a)] and switches to linear field dependency beyond 50 kOe, though Mathshira *et al.* [19] report small and positive magnetoresistance at all temperatures. The $x = 0.5$ and 1.0 material shows large negative magnetoresistance, varying quadratically at low fields and switching over to linear dependence beyond 50 kOe. The magnitude of negative magnetoresistance keeps increasing with decrease in temperature and, at 2.25 K and 90 kOe, reaches 28% and 45% in the $x = 0.5$ and 1.0 compounds respectively, shown in Figs. 5(b) and 5(c). The $x = 1.0$ compound shows a

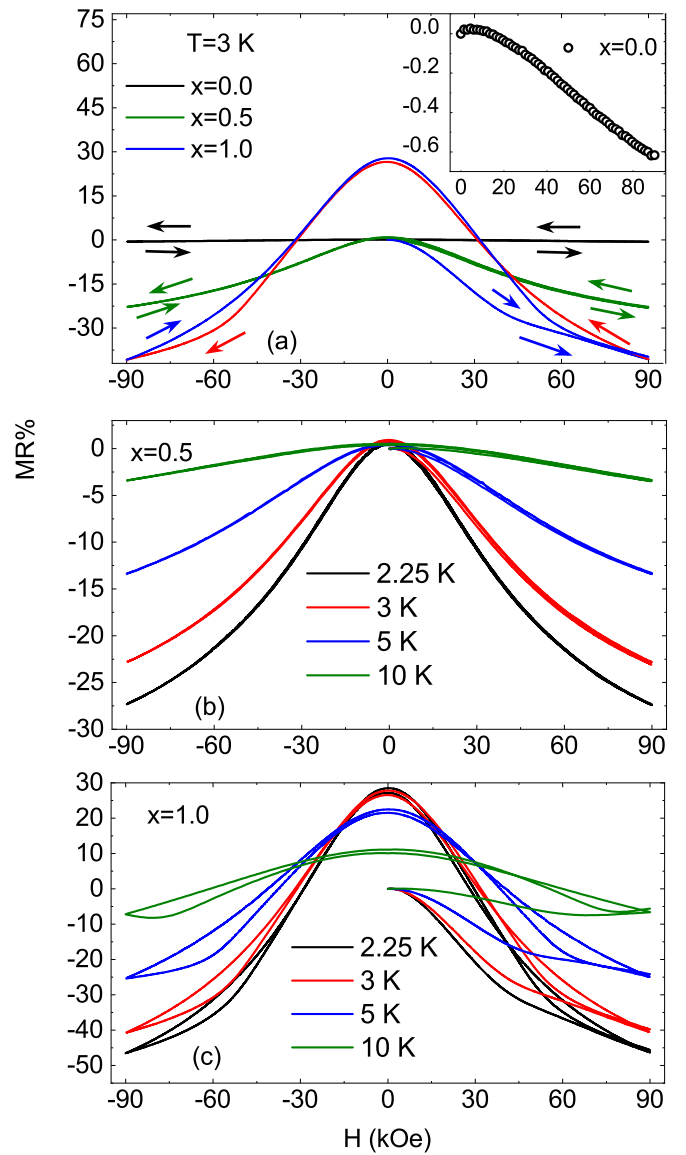


FIG. 5. (a) Magnetic field dependent MR for $(\text{Eu}_{1-x}\text{Nd}_x)_2\text{Ir}_2\text{O}_7$, where $x = 0, 0.5$, and 1.0 , at 3 K with field -90 to $+90$ kOe. Inset: close view of the field dependent MR for $x = 0.0$. (b), (c) Magnetic field dependent MR for the $x = 0.5$ and 1.0 compounds at different temperatures.

hysteresis loop between the first up and down sweeps of the field. This hysteresis loop in MR for $x = 1.0$ is also accompanied by a tiny hysteresis in the isothermal magnetization data. It is clear that negative magnetoresistance increases dramatically only with incorporation of the Nd moment and its interaction ($f - d$ exchange) with Ir electrons.

Another feature, i.e., the increase of resistance when the magnetic field is cycled back to zero field, as shown in Fig. 6, is proportional to the magnitude of the magnetic field cycle. This is explained in Sec. IV.

Figures 7(a)–7(c) show the temperature variation of the heat capacity in the temperature ranges 2.1–150 K, 2.1–130 K, and 2.1–60 K for the $x = 0.0, 0.5$, and 1.0 compounds, respectively, during warming. We observe that there is no anomaly at the T_{irr} for the $x = 0.0$ and 0.5 compounds, though the

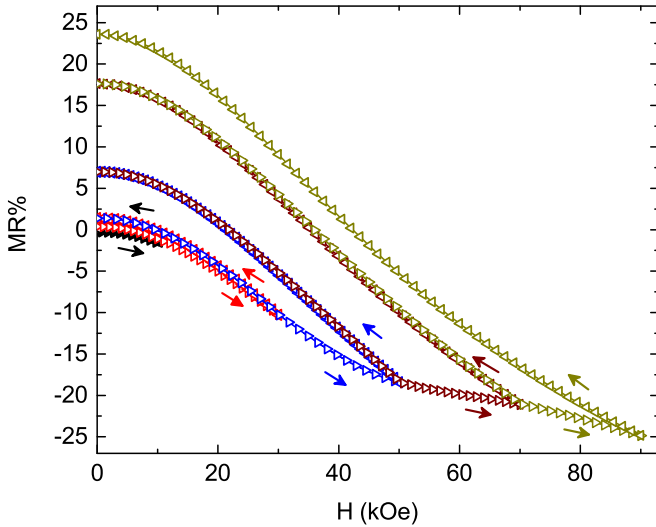


FIG. 6. Different magnetic field cycling MR at 5 K for the compound $(\text{Eu}_{1-x}\text{Nd}_x)_2\text{Ir}_2\text{O}_7$, where $x = 1.0$.

$x = 1.0$ compound shows a faint anomaly at 35 K. The inset in Fig. 7(a) shows the C/T vs T^2 data for the $x = 0.0$ compound. We get an excellent fit to the specific heat within the temperature region 2.1–6 K by assuming

$$C = \gamma T + \beta T^3. \quad (2)$$

The fitting parameters γ and β are $31.8 \text{ mJ mol}^{-1} \text{ K}^{-2}$ and $0.954 \text{ mJ mol}^{-1} \text{ K}^{-4}$. The γ value is close to the $33 \text{ mJ mol}^{-1} \text{ K}^{-2}$ reported by Ishikawa *et al.* [15]. It is important

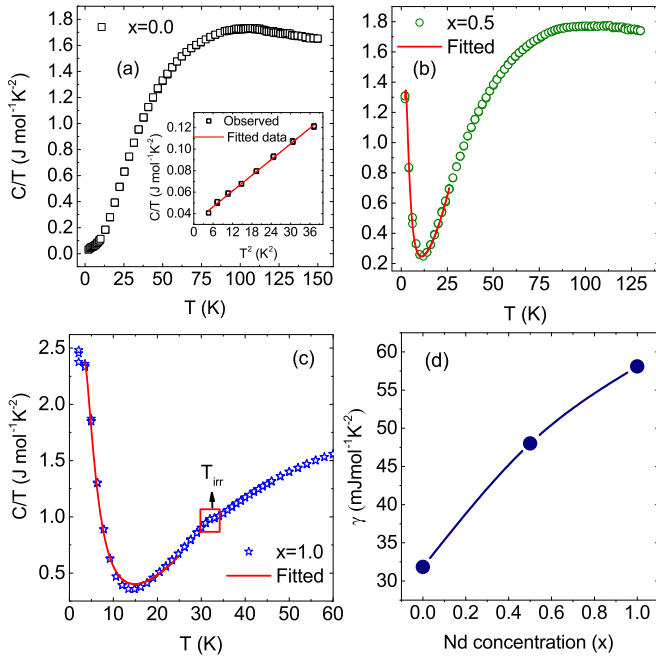


FIG. 7. (a)–(c) Zero field specific heat (C/T) as a function of temperature between different temperature ranges for the $x = 0.0$, 0.5, and 1.0 compound, respectively, and the solid lines are the fitting data. The inset in (a) shows C/T vs T^2 data at low temperature for the $x = 0.0$ compound. (d) Variation of γ with Nd doping.

to point out that a linear in temperature term is absolutely necessary to fit the data at lower temperatures ($T < 30 \text{ K}$). This is surprising because in that temperature region, the resistivity is nonmetallic. Weakly localized Fermi liquids can give linear specific heat because of the finite density of states near the Fermi energy, but the resistivity of the parent compound does not follow $\frac{1}{T^{0.5}}$ for a three-dimensional dirty metal. In strongly localized Fermi systems (that show variable-range hopping type of conductivity), specific heat comes purely from spin degrees of freedom and is not linear. Moreover, in the strong localization limit, spin susceptibility does not follow the Curie-Weiss form as we observe. Dirac or Weyl fermions with linear energy dispersion give a T^3 specific heat. Spin waves (bosons) about an antiferromagnetically ordered state also do not give linear specific heat. We shall comment on it in Sec. IV.

In Figs. 7(b) and 7(c), we see an anomalous increase of specific heat at low temperatures, in both the $x = 0.5$ and 1.0 compounds, that looks like a Schottky-type anomaly. We get a good fit by assuming [40]

$$C = \gamma T + \beta T^3 + n \left(\frac{\Delta_0}{T} \right)^2 \frac{\exp(\Delta_0/T)}{[1 + \exp(\Delta_0/T)]^2}, \quad (3)$$

where n and Δ_0 are proportional to the number of two-level systems and the energy separation between the two levels, respectively.

The fitting parameters γ , β , n , and Δ_0 for the $x = 0.5$ and 1.0 compounds are $48 \text{ mJ mol}^{-1} \text{ K}^{-2}$, $0.945 \text{ mJ mol}^{-1} \text{ K}^{-4}$, 8.2 and 7.83 K (0.67 meV) and $58.1 \text{ mJ mol}^{-1} \text{ K}^{-2}$, $0.907 \text{ mJ mol}^{-1} \text{ K}^{-4}$, 19.82 and 10.35 K (0.89 meV), respectively. We note that the value of Δ_0 is very similar to the reported value obtained using inelastic neutron scattering (i.e., 1.3 meV) [25,41]. Coefficient γ increases with Nd doping, but β does not vary much. Both the number of degrees of freedom n and energy separation between the two levels Δ_0 increases with Nd doping. We suggest that the Schottky anomaly occurs because of an effective molecular field H_{mf} via the $f-d$ exchange interaction present at the Nd sites once the weak AIAO antiferromagnetic transition of the Ir moments sets in, as suggested earlier for this system [25,41]. Nd^{3+} is a Kramer ion, and H_{mf} splits the ground-state doublet of each Nd^{3+} at low temperature. If the effective moment of Nd^{3+} is μ_{Nd} , then $\Delta_0 = 2\mu_{Nd} H_{mf}$. There will be some additional contribution to H_{mf} from the Nd-Nd superexchange interaction in a mean-field sense.

Figure 8(b) shows that the peak (Schottky) temperature progressively shifts towards higher temperature (i.e., Δ_0 increases with applied magnetic field) and the peak height decreases due to an increase in ordering (decrease in entropy) as we increase the external magnetic field from 0.0 to 90 kOe. This is typical of a Schottky peak coming from localized two-level systems of spin origin (Nd moment).

More interesting is the magnetic field dependence of the linear specific-heat coefficient γ for $x = 1.0$. Figure 8(a) shows that in an $x = 0.0$ material, γ does not vary with the magnetic field, as was observed earlier in a spin-1/2 gapless spin liquid [42,43]. In an $x = 1.0$ material, on the other hand, γ varies superlinearly with the magnetic field beyond 30 kOe and shows no sign of saturation even at 90 kOe [see the inset

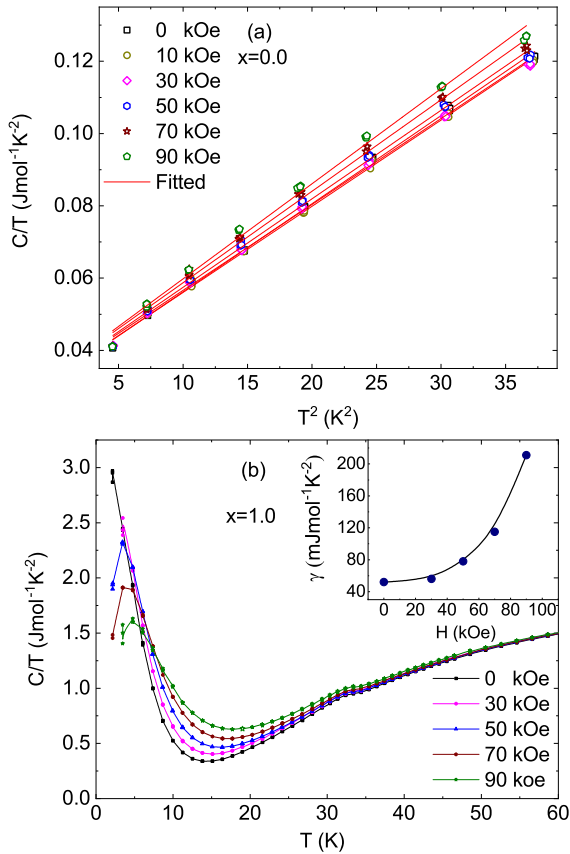


FIG. 8. (a) C/T vs T^2 data with different field for the $x = 0.0$ compound with fitting. (b) Magnetic field dependent specific heat as a function of temperature for the $x = 1.0$ compound. Inset: Field dependent γ .

in Fig. 8(b)]. Both linear specific heat and its curious variation with magnetic field were not seen before in pyrochlore iridate compounds, and in Sec. IV, we point out the possible origin.

IV. DISCUSSION

The physics of pyrochlore iridates is dictated by $5d$ electrons of Ir, which has strong spin-orbit coupling and a moderate Hubbard repulsion U (due to the large spatial extent of $5d$ orbitals). The combined effect of the octahedral crystal field of oxygen anions and spin-orbit coupling leads to an effective single-band (half-filled) description in terms of pseudospin (spin-orbit entangled) $J_{\text{eff}} = 1/2$ states.

Resistivity, as we have already discussed, has two main problems: (1) inherent disorder due to the interchange of rare-earth and transition metal sites, and any other off-stoichiometry due to oxygen concentration, and (2) the observation of domain formation and lower resistance in the domain boundary region than in the bulk. Therefore, transport measurements do not reflect precise electronic states in the bulk.

Both Ir and Nd ion sublattices are a pyrochlore lattice. The superexchange interaction between Ir-Ir and Nd-Nd moments is antiferromagnetic. Moreover, due to spin-orbit coupling, both Ir and Nd pseudospin $1/2$'s have single-ion anisotropy along the local $[111]$ axis (towards the center of tetrahedras).

The ground state of such a model is AIAO ordering for both Ir and Nd moments. The $f - d$ exchange interaction has been derived theoretically [18]. It is seen that the $f - d$ interaction is such that a local AIAO ordering of the Ir moment gives an effective magnetic field at the Nd moment sites, encouraging AOAI ordering of Nd moments. The reason for magnetic irreversibility (field-induced moment) is puzzling. It is true that the magnetic field can destabilize AIAO ordering and lead to three-in-one-out or two-in-two-out states because their energies might be very close to the AIAO magnetic state. All these states have a net moment per tetrahedra (unlike in the AIAO state), but these net moments must alternate going from one tetrahedra to the next, and an increase in magnetization induced by the magnetic field is not expected. We suggest that the induced moment comes because of inherent disorder of the kind we mentioned before. Suppose a few Ir and Eu ions switch sites (interchange) in $\text{Eu}_2\text{Ir}_2\text{O}_7$. Then, if an Eu^{3+} ion (zero net pseudospin) sits at an Ir site, the Ir moments in all tetrahedras connected to this site will deviate from AIAO ordering, i.e., those tetrahedras will pick up a net magnetic moment. Second, an Ir electron from a near-neighbor site can now hop into an empty $5d$ orbital of the Eu or Nd ions (delocalization of Ir electrons through Eu/Nd on Ir sublattice sites), creating an effective double exchange type local ferro-correlation along with a net moment.

As the material cools down from a high temperature, the Ir-Ir superexchange and magnetic anisotropy slowly take over and the Ir moments start ordering (AIAO) below $T = 120$ K, though the observed magnitude of AIAO ordered Ir moments is very small [25]. The AIAO ordering of Ir moments gives an effective magnetic field at Nd moment sites. This is visible from the observed Schottky peak in the specific-heat data for the $x = 0.5$ and 1.0 compounds. However, the inverse susceptibility tending towards a zero value in Figs. 4(a)–4(c) indicates a paramagnetic background at low temperature.

It has been argued [44] that real-space spin chirality, defined as $\chi_{ijk} = \mathbf{S}_i \cdot \mathbf{S}_j \times \mathbf{S}_k$, is responsible for the negative magnetoresistance. Spin chirality [45] can be written in terms of the underlying electron operators (fermions) as $\frac{1}{2}\chi_{ijk} = P_{ijk} - P_{ikj}$, where $P_{ijk} = \chi_{ij}\chi_{jk}\chi_{ki}$ and $\chi_{ij} = C_{i\sigma}^\dagger C_{j\sigma}$, where C 's are electron operators. A nonzero value of χ_{ijk} leads to a Berry phase picked up by electrons as it circulates around a triangular plaquette, i.e., as if spin chirality creates a fictitious magnetic field perpendicular to the plaquette. This chirality has to be contrasted with the chirality of Weyl fermions near Weyl points, which are created by a singular Berry phase in momentum space [46]. This kind of real-space spin chirality can give the Hall effect without a magnetic field as observed in MnSi [47] and negative magnetoresistance [48]. When the spin chirality of all triangular plaquettes is staggered or along a random direction, the magnetoresistance varies quadratically with the magnetic field. At a higher magnetic field, when the chirality of most triangular plaquettes is preferably aligned along some direction, the asymmetric scattering of electrons by spin chirality can occur and one gets odd-parity magnetoresistance, i.e., magnetoresistance varying linearly with the magnetic field. Therefore, the magnetic ordering of the Ir electrons can be thought of as a weak antiferromagnetic (AIAO) long-range ordering (reported earlier by RXD and

μ SR measurement [28,37]) superimposed on a chiral spin-liquid state [8,49–51].

A huge increase in magnetoresistance with an increase in Nd points out the importance of Nd moments. We suggest that apart from the scattering of carriers in the domain walls by chirality fluctuations, there is an additional Kondo scattering of carriers by Nd electron moments. Kondo scattering in heavy fermion materials gives quadratic field dependent at low field and linear at high field negative magnetoresistance [52]. For Nd doping, the resistance value increases after a field cycle due to reduction of the domain wall, i.e., in between either AIAO-AOAI, or vice versa, ordered regions [34]. This was noticed before in $\text{Pr}_2\text{Ir}_2\text{O}_7$ [53] and in $\text{Nd}_2\text{Ir}_2\text{O}_7$ [14].

Now we come to our observation of linear specific heat in all three samples at the low-temperature insulating phase. This is most unusual. Linear specific heat can occur in a Fermi system in a weak localization regime because of the nonzero density of states near the Fermi energy, but as we discussed earlier, the temperature-dependent resistivity rules out weak localization. Weyl fermions show nonmetallic resistivity (negative temperature coefficient of resistivity), but, because of their linear dispersion, Weyl fermions would rather give a T^3 specific heat. Antiferromagnets in frustrated lattices often give spin-liquid ground states supporting exotic excitations called spinons obeying fractional quantum statistics [54]. Theoretical [55] analysis of the kagome lattice antiferromagnet suggests that a linear specific heat in an insulating antiferromagnet is possible if spinons have a finite-area Fermi surface. Spin liquids are like spin superfluids (pairing between spinons of opposite spins) with or without a gap for spinon excitations [56]. Free spinons give a linear specific heat. In an $x = 0.0$ material, γ does not change with the magnetic field and this is consistent with a spin-liquid state having gapless spinon excitations [42,43] coexisting with long-range antiferromagnetic ordering [37], as is observed in other magnetically ordered systems [49–51]. The magnitude of γ in an $x = 1.0$ compound is also much larger (this is due to the contribution of spinons from both the Ir and Nd sublattices) than in an $x = 0.0$ compound in the zero field. It is also possible that the Nd spin system develops a spin-liquid kind of singlet formation due to $f - d$ exchange interaction. The $f - d$ exchange interaction gets modified beyond a certain applied magnetic field, which induces breaking of Nd and Ir spin singlets. Hence, in $x = 1.0$, γ varies superlinearly beyond a certain magnetic field and does not show any sign of saturation even at 90 kOe [see

inset of Fig. 8(b)]. This suggests that spin-liquid type singlet correlation is in both Ir and Nd spin subsystems without affecting the long-range antiferromagnetic ordering. Here we would like to point out categorically that there is a coexistence of Neel order (AIAO) [24,29] and singlet spin-liquid order (i.e., long-range resonating valence bond ordering) [49–51]. It needs more experimental investigation of two pyrochlore antiferromagnets coupled by $f - d$ exchange.

V. CONCLUSION

From different magnetic field cycling MR, it is clear that these materials are fragmented into domains with larger resistivity (larger charge gap) separated by domain walls with lesser resistivity (lesser charge gap). From our analysis of magnetic susceptibility, low-temperature linear specific heat, and negative magnetoresistance with low-field quadratic and high-field linear dependence, we conclude that the magnetic state of Ir electrons in the domains (larger volume fraction) is very weak antiferromagnetic AIAO ordering superimposed on a predominantly possible chiral spin-liquid state, i.e., coexistence of AIAO ordering and chiral spin liquid. Observation of linear specific heat in the insulating low-temperature phase rules out the possibility of a Weyl semimetal phase in these materials. Linear specific heat comes from spinons, which are excitations above the spin-liquid state. We also conclude that $f - d$ exchange interaction encourages singlet correlation (spinon pairing). Transport properties such as resistivity and magnetoresistance come from the domain-wall regions, where small AIAO ordering of Ir moments is destroyed, leading to smaller charge gap than in the domains. In an $x = 0.0$ material, this chiral spin liquid gives very small negative magnetoresistance. In $x = 0.5$ and 1.0 materials, magnetoresistance is hugely amplified by Kondo scattering of rare-earth moments with the chiral spin liquid. Chiral spin liquid along with Kondo scattering could be exciting areas that might lead to new physics.

ACKNOWLEDGMENTS

S.M. would like to thank Anish Karmahapatra, ECMP Division, SINP for XRD measurements. This work is partially supported by SERB, GOI under the TARE project (File No. TAR/2018/000546).

-
- [1] O. Vafek and A. Vishanath, *Annu. Rev. Condens. Matter Phys.* **5**, 83 (2014)
 [2] W. Witczek-Krempa, G. Chen, Y. B. Kim, and L. Balents, *Annu. Rev. Condens. Matter Phys.* **5**, 57 (2014); T. Bau, M. Z. Hasan, and C. L. Kane, *Rev. Mod. Phys.* **82**, 3045 (2010); X. L. Qi and S. C. Zhang, *ibid.* **83**, 1057 (2011).
 [3] Z. K. Liu, B. Zhou, Y. Zhang, Z. J. Wang, H. M. Weng, O. Prabhakaran, S. K. Mo, Z. X. Shen, Z. Fang, X. Dai, Z. Hussain and Y. L. Chen, *Science* **343**, 864 (2014); M. Neupane, S.-Y. Xu, R. Sankar, N. Alidoust, Guang Bian, Chang Liu, I. Belopolski, T.-R. Chang, H.-T. Jeng, H. Lin, A. Bansil, F. Chou,

- and M. Zahid Hasan, *Nat. Commun.* **5**, 3786 (2014); S. Y. Xu, C. Liu, I. Belopolski, S. K. Kushwaha, R. Sankar, J. W. Krizan, T. R. Chang, C. M. Polley, J. Adell, T. Balasubramanian, K. Miyamoto, N. Alidoust, G. Bian, M. Neupane, H. T. Jeng, C. Y. Huang, W. F. Tsai, T. Okuda, A. Bansil, F. C. Chou, R. J. Cava, H. Lin, and M. Z. Hasan, *Phys. Rev. B* **92**, 075115 (2015); S. Borisenko, Q. Gibson, Danil Evtushinsky, V. Zabolotnyy, B. Buchner, and R. J. Cava, *Phys. Rev. Lett.* **113**, 027603 (2014).
 [4] B. Q. Lv, N. Xu, H. M. Weng, J. Z. Ma, P. Richard, X. C. Huang, L. X. Zhao, G. F. Chen, C. E. Matt, F. Bisti, V. N. Strocov, J.

- Mesot, Z. Fang, X. Dai, T. Qian, M. Shi, and H. Ding, *Nat. Phys.* **11**, 724 (2015); S.-Y. Xu *et al.*, *ibid.* **11**, 748 (2015).
- [5] X. Wan, A. M. Turner, A. Vishwanath, and S. Y. Savrasov, *Phys. Rev. B* **83**, 205101 (2011).
- [6] T. Ohtsukia, Z. Tian, A. Endoa, M. Halima, S. Katsumotoa, Y. Kohamaa, K. Kindoa, M. Lippmaa, and S. Nakatsuji, *Proc. Natl. Acad. Sci.* **116**, 8803 (2019).
- [7] D. T. Son and B. Z. Spivak, *Phys. Rev. B* **88**, 104412 (2013).
- [8] Y. Machida, S. Nakatsuji, S. Onoda, T. Tayama, and T. Sakakibara, *Nature (London)* **463**, 210 (2010).
- [9] D. Pesin and L. Balents, *Nat. Phys.* **6**, 376 (2010).
- [10] S. Nakatsuji, Y. Machida, Y. Maeno, T. Tayama, T. Sakakibara, J. van Duijn, L. Balicas, J. N. Millican, R. T. Macaluso, and J. Y. Chan, *Phys. Rev. Lett.* **96**, 087204 (2006).
- [11] B. J. Kim, H. Ohsumi, T. Komesu, S. Sakai, T. Morita, H. Takagi, and T. Arima, *Science* **323**, 1329 (2009); Y.-Z. You, I. Kimchi, and A. Vishwanath, *Phys. Rev. B* **86**, 085145 (2012).
- [12] H. Zhang, K. Haule, and D. Vanderbilt, *Phys. Rev. Lett.* **118**, 026404 (2017).
- [13] D. Yanagishima and Y. Maeno, *J. Phys. Soc. Jpn.* **70**, 2880 (2001).
- [14] K. Matsuhira, M. Wakeshima, Y. Hinatsu, and S. Takagi, *J. Phys. Soc. Jpn.* **80**, 094701 (2011).
- [15] J. J. Ishikawa, E. C. T. O'Farrell, and S. Nakatsuji, *Phys. Rev. B* **85**, 245109 (2012).
- [16] A. B. Sushkov, J. B. Hofmann, G. S. Jenkins, J. Ishikawa, S. Nakatsuji, S. Das Sarma, and H. D. Drew, *Phys. Rev. B* **92**, 241108(R) (2015).
- [17] F. F. Tafti, J. J. Ishikawa, A. McCollam, S. Nakatsuji, and S. R. Julian, *Phys. Rev. B* **85**, 205104 (2012).
- [18] G. Chen and M. Hermele, *Phys. Rev. B* **86**, 235129 (2012).
- [19] K. Matsuhira, A. Tokunaga, M. Wakeshima, Y. Hinatsu, and S. Takagi, *J. Phys. Soc. Jpn.* **82**, 023706 (2013).
- [20] T. Hasegawa, N. Ogita, K. Matsuhira, S. Takagi, M. Wakeshima, Y. Hinatsu, and M. Udagawa, *J. Phys.: Conf. Ser.* **200**, 012054 (2010).
- [21] K. Ueda, J. Fujioka, Y. Takahashi, T. Suzuki, S. Ishiwata, Y. Taguchi, and Y. Tokura, *Phys. Rev. Lett.* **109**, 136402 (2012).
- [22] Z. Tian, Y. Kohama, T. Tomita, H. Ishizuka, T. H. Hsieh, J. J. Ishikawa, K. Kindo, L. Balents, and S. Nakatsuji, *Nat. Phys.* **12**, 134 (2016).
- [23] M. Nakayama, T. Kondo, Z. Tian, J. J. Ishikawa, M. Halim, C. Bareille, W. Malaeb, K. Kuroda, T. Tomita, S. Ideta, K. Tanaka, M. Matsunami, S. Kimura, N. Inami, K. Ono, H. Kumigashira, L. Balents, S. Nakatsuji, and S. Shin, *Phys. Rev. Lett.* **117**, 056403 (2016).
- [24] H. Guo, C. Ritter, and A. C. Komarek, *Phys. Rev. B* **94**, 161102(R) (2016).
- [25] K. Tomiyasu, K. Matsuhira, K. Iwasa, M. Watahiki, S. Takagi, and M. Wakeshima, *J. Phys. Soc. Jpn.* **81**, 034709 (2012).
- [26] K. Ueda, J. Fujioka, B.-J. Yang, J. Shiozai, A. Tsukazaki, S. Nakamura, S. Awaji, N. Nagaosa, and Y. Tokura, *Phys. Rev. Lett.* **115**, 056402 (2015).
- [27] H.-J. Koo, M. H. Whangbo, and B. J. Kennedy, *J. Solid State Chem.* **136**, 269 (1998).
- [28] S. Zhao, J. M. Mackie, D. E. MacLaughlin, O. O. Bernal, J. J. Ishikawa, Y. Ohta, and S. Nakatsuji, *Phys. Rev. B* **83**, 180402(R) (2011).
- [29] S. M. Disseler, C. Dhital, T. C. Hogan, A. Amato, S. R. Giblin, C. de la Cruz, A. Daoud-Aladine, S. D. Wilson, and M. J. Graf, *Phys. Rev. B* **85**, 174441 (2012); H. Guo, K. Matsuhira, I. Kawasaki, M. Wakeshima, Y. Hinatsu, I. Watanabe, and Zhuan Xu, *ibid.* **88**, 060411(R) (2013).
- [30] W. Witczak-Krempa and Y. B. Kim, *Phys. Rev. B* **85**, 045124 (2012).
- [31] P. Telang, K. Mishra, A. K. Sood, and S. Singh, *Phys. Rev. B* **97**, 235118 (2018).
- [32] A. Banerjee, J. Sannigrahi, S. Giri, and S. Majumdar, *Phys. Rev. B* **96**, 224426 (2017).
- [33] Z. Porter, E. Zoghlin, S. Britner, S. Husremovic, J. P. C. Ruff, Y. Choi, D. Haskel, G. Laurita, and S. D. Wilson, *Phys. Rev. B* **100**, 054409 (2019).
- [34] E. Y. Ma, Y. T. Cui, K. Ueda, S. Tang, K. Chen, N. Tamura, P. M. Wu, J. Fujioka, Y. Tokura, and Z.-X. Shen, *Science* **350**, 538 (2015).
- [35] H.-Z. Lu and S.-Q. Shen, *Phys. Rev. B* **92**, 035203 (2015).
- [36] A. Malinowska, M. Z. Cieplaka, M. Berkowska, and S. Guha, *Acta Physica Polonica A* **109**, 611 (2006); N. Mott, *Conduction in Non-Crystalline Materials* (Clarendon, Oxford, 1993).
- [37] H. Sagayama, D. Uematsu, T. Arima, K. Sugimoto, J. J. Ishikawa, E. O'Farrell, and S. Nakatsuji, *Phys. Rev. B* **87**, 100403(R) (2013).
- [38] Y. Takikawa, S. Ebisu, and S. Nagata, *J. Phys. Chem. Solids* **71**, 1592 (2010).
- [39] A. Bertin, P. D. de Reotier, B. Fak, C. Martin, A. Yaouanc, A. Forget, D. Sheptyakov, B. Frick, C. Ritter, A. Amato, C. Baines, and P. J. C. King, *Phys. Rev. B* **92**, 144423 (2015).
- [40] N. Ghosh, U. K. Roßler, K. Nenkov, C. Hucho, H. L. Bhat, and K.-H. Müller, *J. Phys.: Condens. Matter* **20**, 395219 (2008).
- [41] M. Watahiki, K. Tomiyasu, K. Matsuhira, K. Iwasa, M. Yokoyama, S. Takagi, M. Wakeshima, and Y. Hinatsu, *J. Phys.: Conf. Ser.* **320**, 012080 (2011).
- [42] S. Yamashita, Y. Nakazawa, M. Oguni, Y. Oshima, H. Nojiri, Y. Shimizu, K. Miyagawa, and K. Kanoda, *Nat. Phys.* **4**, 459 (2008).
- [43] S. Yamashita, T. Yamamoto, Y. Nakazawa, M. Tamura, and R. Kato, *Nat. Commun.* **2**, 275 (2011).
- [44] T. C. Fujita, Y. Kozuma, M. Uchida, A. Tsukazaki, T. Arima, and M. Kawasaki, *Sci. Rep.* **5**, 9711 (2015).
- [45] X. G. Wen, F. Wilczek, and A. Zee, *Phys. Rev. B* **39**, 11413 (1989).
- [46] N. Nagaosa, X. Z. Yu, and Y. Tokura, *Philos. Trans. A: Math. Phys. Eng. Sci.* **370**, 5806 (2012).
- [47] Y. Taguchi, Y. Oohara, H. Yoshizawa, N. Nagaosa, and Y. Tokura, *Science* **291**, 2573 (2001).
- [48] A. Neubauer, C. Pfleiderer, B. Binz, A. Rosch, R. Ritz, P. G. Niklowitz, and P. Boni, *Phys. Rev. Lett.* **102**, 186602 (2009).
- [49] T. Nagata, H. Fujino, K. Ohishi, J. Akimitsu, S. Katano, M. Nishi, and K. Kakurai, *J. Phys. Chem. Solids* **60**, 1039 (1999).
- [50] A. Zorko, M. Pregelj, M. Klanjšek, M. Gomilšek, Z. Jagličić, J. S. Lord, J. A. T. Verezhak, T. Shang, W. Sun, and J.-X. Mi, *Phys. Rev. B* **99**, 214441 (2019).
- [51] E. M. Kenney, C. U. Segre, W. Lafargue-Dit-Hauret, O. I. Lebedev, M. Abramchuk, A. Berlie, S. P. Cottrell, G. Simutis, F. Bahrami, N. E. Mordvinova, G. Fabbri, J. L. McChesney, D.

- Haskel, X. Rocquefelte, M. J. Graf, and F. Tafti, *Phys. Rev. B* **100**, 094418 (2019).
- [52] A. C. Hewson, *The Kondo Problems of Heavy Fermions* (Cambridge University Press, Cambridge, 1993).
- [53] L. Balicas, S. Nakatsuji, Y. Machida, and S. Onoda, *Phys. Rev. Lett.* **106**, 217204 (2011); T.-H. Han, R. Chisnell, C. J. Bonnoit, D. E. Freedman, V. S. Zapf, N. Harrison, D. G. Nocera, Y. Takano, and Y. S. Lee, [arXiv:1402.2693](https://arxiv.org/abs/1402.2693).
- [54] L. Balents, *Nature (London)* **464**, 199 (2010).
- [55] Y. Ran, M. Hermele, P. A. Lee, and X. G. Wen, *Phys. Rev. Lett.* **98**, 117205 (2007).
- [56] G. Baskaran, Z. Zou, and P. W. Anderson, *Solid. State Commun.* **63**, 973 (1987).